Analytica Chimica Acta 701 (2011) 75–80

Contents lists available at ScienceDirect

Analytica Chimica Acta

journal homepage: www.elsevier.com/locate/aca

An ultrasensitive hydrogen peroxide biosensor based on electrocatalytic synergy of graphene–gold nanocomposite, CdTe–CdS core–shell quantum dots and gold nanoparticles

Gu Zhiguo[a], Yang Shuping[a], Li Zaijun[a,*], Sun Xiulan[b], Wang Guangli[a], Fang Yinjun[c], Liu Junkang[a]

[a] School of Chemical and Material Engineering, Jiangnan University, Wuxi 214122, PR China
[b] School of Food Science and Technology, Jiangnan University, Wuxi 214122, PR China
[c] Zhejiang Zanyu Technology Co., Ltd., Hangzhou 310009, PR China

GRAPHICAL ABSTRACT

We first reported an ultrasensitive hydrogen peroxide biosensor in this work, which was fabricated by coating graphene–gold nanocomposite, CdTe–CdS core–shell quantum dots, gold nanoparticles and horseradish peroxidase in sequence on the surface of gold electrode. Since a promising their electrocatalytic synergy towards hydrogen peroxide was achieved, the biosensor displayed very high sensitivity, low detection limit ($S/N = 3$) (3.2×10^{-11} M) and good long-term stability (20 weeks).

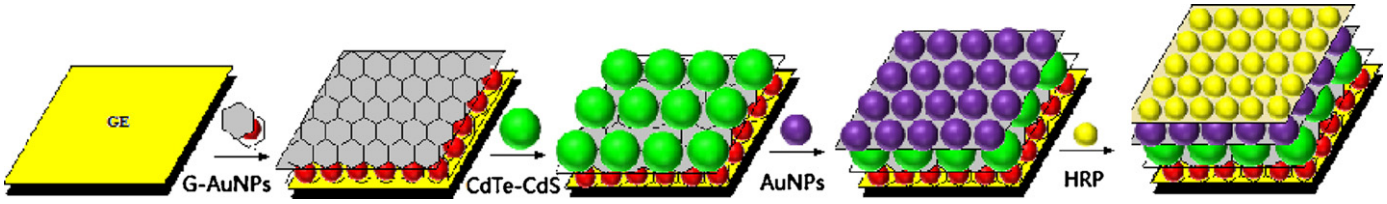

HIGHLIGHTS

- We for the first time integrated novel hydrogen peroxide biosensor based on G–AuNP, CdTe–CdS and AuNPs.
- Three nanomaterials show remarkable synergistic electrocatalysis towards hydrogen peroxide.
- The biosensor provides the best sensitivity in all biosensors based on graphene for detection of glucose up to now.

ARTICLE INFO

Article history:
Received 21 April 2011
Received in revised form 8 June 2011
Accepted 9 June 2011
Available online 4 July 2011

Keywords:
Graphene–gold nanocomposite
CdTe–CdS core–shell quantum dots
Gold nanoparticles
Biosensor
Hydrogen peroxide

ABSTRACT

We first reported an ultrasensitive hydrogen peroxide biosensor in this work. The biosensor was fabricated by coating graphene–gold nanocomposite (G–AuNP), CdTe–CdS core–shell quantum dots (CdTe–CdS), gold nanoparticles (AuNPs) and horseradish peroxidase (HRP) in sequence on the surface of gold electrode (GE). Cyclic voltammetry and differential pulse voltammetry were used to investigate electrochemical performances of the biosensor. Since promising electrocatalytic synergy of G–AuNP, CdTe–CdS and AuNPs towards hydrogen peroxide was achieved, the biosensor displayed a high sensitivity, low detection limit ($S/N = 3$) (3.2×10^{-11} M), wide calibration range (from 1×10^{-10} M to 1.2×10^{-8} M) and good long-term stability (20 weeks). Moreover, the effects of omitting G–AuNP, CdTe–CdS and AuNP were also examined. It was found that sensitivity of the biosensor is more 11-fold better if G–AuNP, CdTe–CdS and AuNPs are used. This could be ascribed to improvement of the conductivity between graphene nanosheets in the G–AuNP due to introduction of the AuNPs, ultrafast charge transfer from

* Corresponding author at: School of Chemical and Material Engineering, Jiangnan University, Wuxi 214122, PR China. Tel.: +86 5105811863; fax: +86 5105811863.
E-mail address: zaijunli@263.net (L. Zaijun).

0003-2670/$ – see front matter
doi:10.1016/j.aca.2011.06.015

CdTe–CdS to the graphene sheets and AuNP due to unique electrochemical properties of the CdTe–CdS, and good biocompatibility of the AuNPs for horseradish peroxidase. The biosensor is of best sensitivity in all hydrogen peroxide biosensors based on graphene and its composites up to now.

1. Introduction

Graphene, a one-atom thick and two-dimensional closely packed honeycomb lattice, has received numerous investigations from both experimental and theoretical scientific communities since the experimental observation of single layers [1]. As a counterpart of graphite with well-separated 2D aromatic sheets, graphene possesses high electron mobility under ambient conditions [2] and large specific surface area with low manufacturing cost [3]. These unique properties make graphene as promising additive or supporting component for potential applications in many technological fields such as solar cell [4], lithium-ion battery [5] and ultracapacitor cell [6]. At present, the use of graphene for biosensor received much attention [7]. However, the studies showed single-, few-, and multilayer graphene materials are not of significant advantages over graphite microparticles in electroanalysis due to poor conductivity between graphene nanosheets and biocompatibility [8]. To date, graphene–metal nanocomposite has become a hot research topic in material science because the hybridization can be an effective strategy to enhance functionality of the material [9], and the integration of nanomaterials potentially paves new way to enhance their electronic, chemical, and electrochemical properties. Among these, graphene–noble metal nanocomposite has attracted special attention due to remarkable electrochemical properties such as graphene–gold nanocomposite (G–AuNP) [10–12] and graphene–platinum nanocomposite [13]. Many investigations have demonstrated the graphene–noble metal hybrid materials offer better electrocatalytic activity than sole graphene. Moreover, some biocompatible materials, such as gold nanoparticle (AuNPs), chitosan and ionic liquid, were introduced into the modified layers to improve the stability of enzyme [14–16].

Semiconductor quantum dots are quasi zero dimensional materials that have gained a great deal of research interest in the past decade due to their exciting size- and shape-dependent properties. Much effort has been made to synthesize quantum dot materials with band gaps that can be easily tuned by changing their size and shape [17]. These materials are highly luminescent with narrow emission line widths, which have enormous potential applications, including use in biolabeling [18] and nanosensor [19]. However, for better application of quantum dots, efficient charge separation has remained a challenge. To improve the charge transfer of quantum dots, many core–shell nanocrystals such as CdTe–CdS have been synthesized and investigated in the five years, which provide the improvement of photostability, charge carrier and charge transfer dynamics [20,21]. Recently, Wang and co-workers found graphene not only enhances electrochemiluminescent intensity of the quantum dots but also decreases the electrochemiluminescent onset potential with the co-reactant hydrogen peroxide [22].

Considering benefits of the G–AuNP, CdTe–CdS and AuNPs, we have integrated them in a biosensor fabrication to exploit electrocatalytic synergy on the improvement of biosensor characteristics in this study. To the best of our knowledge, such a hydrogen peroxide biosensor has not been reported so far with these integrated components. The biosensor presents high sensitivity, selectivity and long-term stability towards the detection of trace hydrogen peroxide.

2. Experimental

2.1. Chemicals

Horseradish peroxidase (HRP) (250 U mg^{-1}), graphite, 1-mercaptopropionic acid (>99%), $CdCl_2$ (99.99%), tellurium powder (Te) (99.997%), $NaBH_4$ (95%), $HAuCl_4{\cdot}3H_2O$ and chitosan (CS) (85%) were obtained from Sigma–Aldrich Chemical Company (Mainland, China). H_2O_2 (30 wt%) was purchased from Beijing Chemical Reagent Company. A phosphate buffered saline (PBS, pH 7, Na_2HPO_4–KH_2PO_4–NaCl–KCl, 0.01 M) was prepared in the laboratory. The CS solution was prepared by dissolving 0.5 g of the CS in 100 mL of 1.0% (v/v) acetic acid. The AuNPs were synthesized by a method described in Ref. [22]. The CdTe–CdS core–shell quantum dots were prepared by similar method in Ref. [23]. All other reagents employed were of analytical reagent grade or with highest quality and were purchased from Shanghai Chemical Company (Shanghai, China), and ultra pure water (18.2 ΩM cm) purified from a Milli-Q purification system was used throughout the experiment.

2.2. Apparatus

Electrochemical experiments were performed with an IM6e electrochemical system (ZAHNER Elektrik, German). A conventional three electrode system was used with Ag/AgCl (saturated KCl) electrode as the reference electrode, platinum wire as the counter electrode, and bare or the modified gold electrode (d = 2 mm) as working electrode. Before use, gold electrode was carefully polished to a mirror finish with 1.0-, 0.3-, and 0.05-μm alumina powder in sequence, rinsed thoroughly with pure water between each polishing step, sonicated in ethanol and pure water for 5 min, respectively, and dried with nitrogen. If not mentioned, all potentials given below were relative to Ag/AgCl (saturated KCl) electrode. Electrochemical impedance measurements were performed in 20 mL of a pH 7.0 PBS containing 1.0 mM $K_3[Fe(CN)_6]$/$K_4[Fe(CN)_6]$ (1:1 mixture). The impedance spectra were measured in the frequency range from 10^5 Hz to 1 Hz in a potential of 0.20 V versus Ag/AgCl (saturated KCl), with a voltage amplitude of 5 mV. The impedance Z was expressed in terms of a real (Z') and an imaginary (Z'') component. Impedance signals were recorded after reaction between the electrodes and the unstirred substrate solution for 5 min. All electrochemical experiments were carried out under quiescent conditions.

Transmission electron microscope (TEM) image, Raman spectrum and X-ray diffraction (XRD) patterns were obtained using a JEOL-2100F transmission electron microscope equipped with an INCA X-ray energy dispersive spectrometer, a HR800 Raman microprobe with a 514 nm laser excitation and an X-ray D/max-2200vpc (Rigaku Corporation, Japan) instrument operated at 40 kV and 20 mA and using Cu Kα radiation (k = 0.15406 nm), respectively.

2.3. Synthesis of G–AuNP

Graphene oxide was prepared from natural flake graphite power by the modified Hummers method [24,25]. The graphene oxide (140 mg) and 1.0 mL of $HAuCl_4$ solution (2.5 mM) were transferred into 140 mL of water. After the dispersed solution was sonicated for several hours until it became translucent with no visible particulate

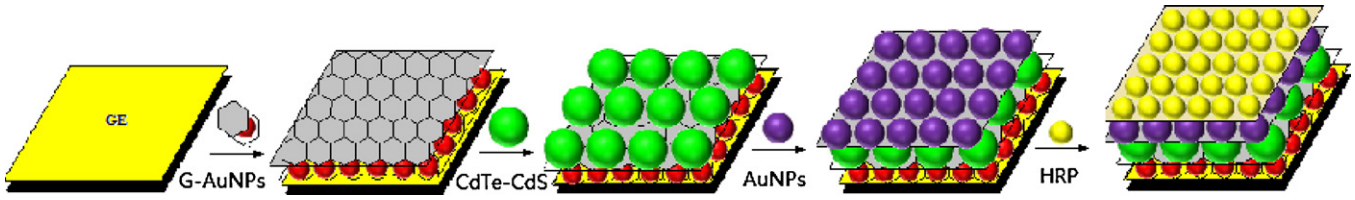

Fig. 1. General procedure for fabrication of HRP/AuNPs /CdTe–CdS/G–AuNP/GE.

matter, it was heated to 100 °C. Then, 2.5 mL of tri-sodium citrate (3.4 mM) and 2.5 mL of $NaBH_4$ solution (50 mM) were added to the above solution with well stirring for 1 h under 100 °C. The resulting G–AuNP was collected by centrifugation, washed with water for three times and dried in a vacuum drier for 24 h.

2.4. Preparation of the biosensor

The G–AuNP was dispersed in the CS solution with a few minutes of ultrasonication to achieve G–AuNP solution (1.0 mg mL^{-1}). After that, the G–AuNP solution (5 μL) was dropped onto the surface of gold electrode and allowed to dry in ambient air for 12 h to obtain G–AuNP-modified electrode. By the same procedure, a 2.5 μL of CdTe–CdS solution (1 mM), 2.5 μL of AuNPs solution (1 mM) and 2.5 μL of the CS solution were cast onto surface of the modified electrode in sequence. Finally, a 5 μL of HRP solution (10 mg mL^{-1}) was cast on the prepared AuNPs/CdTe–CdS/G–AuNP/GE. Right after casting, the biosensor (HRP–AuNPs/CdTe–CdS/G–AuNP/GE) was moved into a refrigerator and kept at 4 °C to dry overnight. During the experiment, the biosensor was stored at 4 °C until use (shown in Fig. 1).

3. Results and discussion

3.1. Characterization of the G–AuNP

During preparation of G–AuNP, the reduction of graphene oxide and deposition of AuNPs on the graphene sheets simultaneously occurred. The as-prepared G–AuNP was well characterized by TEM, electrochemical impedance spectroscopy, XRD and Raman spectrum. As shown in Fig. 2, the AuNPs with particle size of about 10 nm were well separated on the wrinkled graphene sheets. The electron transfer resistance of the redox for the G–AuNP was remarkably lower than that of the sole graphene, indicating that the G–AuNP has better conductivity than the sole graphene. XRD pattern of the G–AuNP includes four sharp diffraction peaks at scattering angles of 38.28°, 44.48°, 64.6° and 77.64°, corresponding to crystal planes (1 1 1), (2 0 0), (2 2 0) and (3 1 1) of gold face-centered cubic crystallographic structure (JCPDS card No. 65-2870). Fig. 2c exhibits a strong *D* line at 1351 cm^{-1}, corresponding to a breathing mode or j-point photons of A_{1g} symmetry, and a relatively weak *G* line at 1581 cm^{-1}, which should be assigned to the in-plane bond-stretching motion of pairs of C sp^2 atoms (the first order scattering

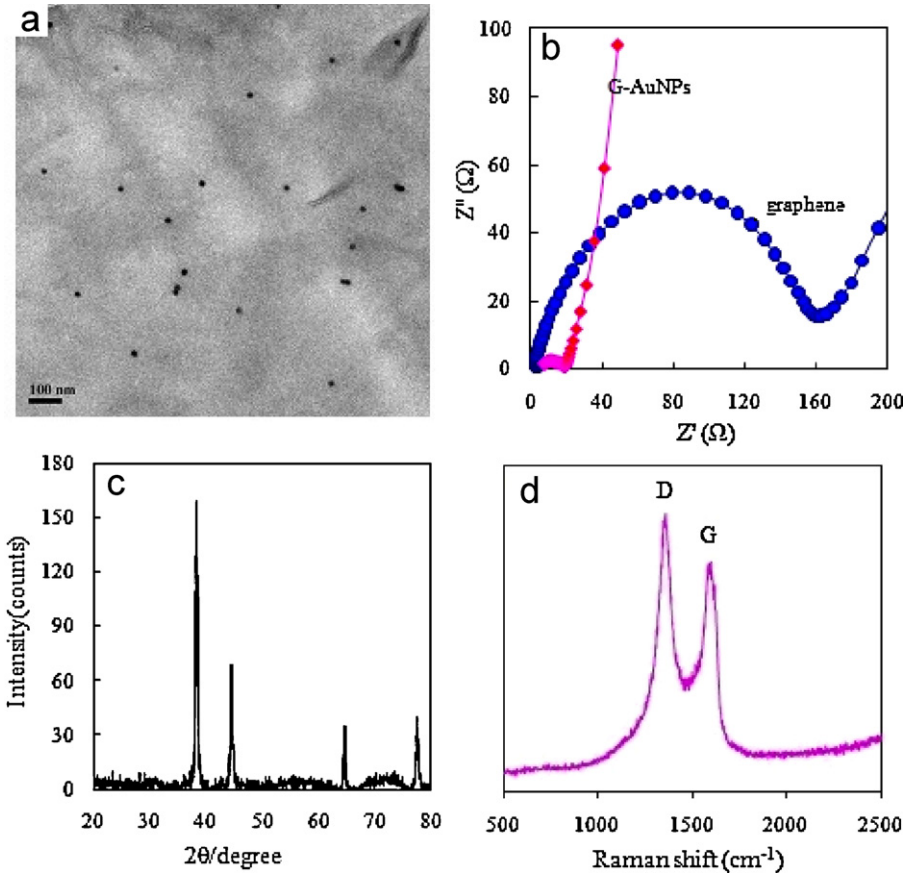

Fig. 2. TEM (a), electrochemical impedance spectrum (b), XRD (c) and Raman spectrum (d) of G–AuNP.

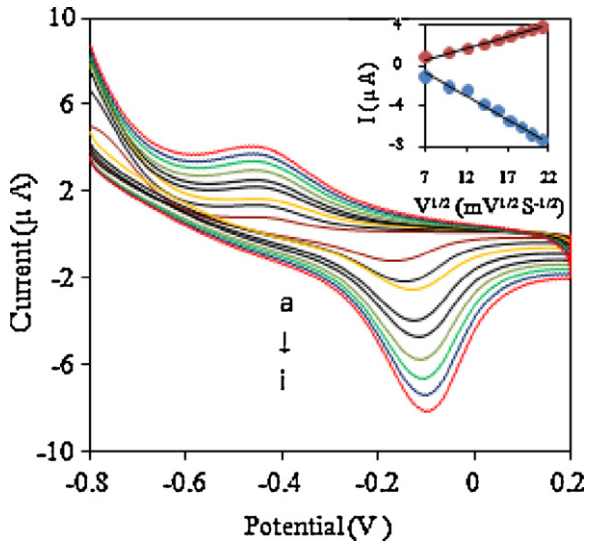

Fig. 3. Cyclic voltammogram of HRP/AuNPs/CdTe–CdS/G–AuNP/GE in PBS (pH 7.0) at 50, 100, 150, 200, 250, 300, 350, 400 and 450 mV s^{-1} (from a to i). Inset: Peak current as a function of different scan rates.

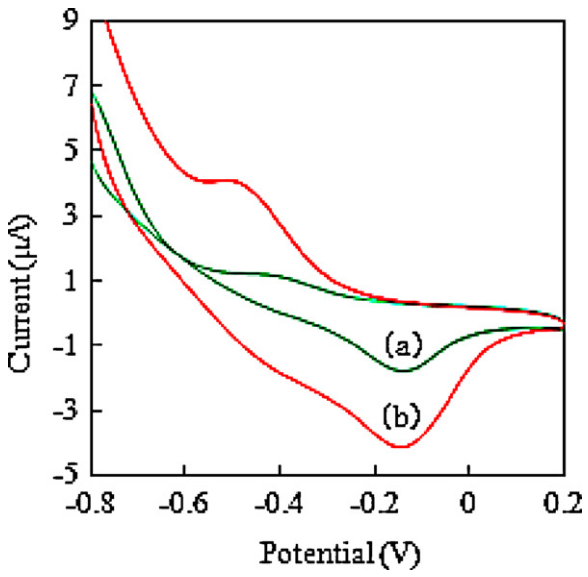

Fig. 4. Cyclic voltammograms of HRP/AuNPs/CdTe–CdS/G–AuNP/GE in the absence hydrogen peroxide (a) and presence of 1×10^{-8} M hydrogen peroxide (b) in pH 7.0 PBS at 100 mV s^{-1}.

of the E_{2g} photons). *D* mode is forbidden in perfect graphite and only becomes active in the presence of disorder, the significant increase of *D*/*G* intensity ratio shows the decrease of the size of the in-plane sp^2 domains and partially disordered crystal structure of graphene nanosheets. Above results demonstrated we successfully obtained a real graphene–gold nanocomposite by in situ synthetic approach.

3.2. Electrochemical properties of the modified electrode

Electrochemical stability of the modified electrode was checked by a repetitive potential sweep at a 100 mV s^{-1} of scan rate. It was found the peak currents almost maintained the same intensity after 100 scans (no shown). The fact exhibits that the modified electrode has fairly good electrochemical stability and the leakage of AuNPs, CdTe–CdS and G–AuNP on the surface of the modified electrode can be neglected. Moreover, the effect of varying scan rate on electrochemical performance of the modified electrode was also examined by cyclic voltammetry (CV). Fig. 3 clearly shows that both the cathodic and anodic peak currents increase with increasing the scan rate and enhancements of both currents are linear to the square root of scan rate, but peak potentials are nearly independent of the scan rate. The above results revealed the electrochemical kinetics was a reversible and diffusion-confined electrochemical process. As the electrochemical measurements were carried out in oxygen saturated PBS solution, the cathodic and anodic peak currents should be assigned to the reduction of oxygen and the oxidization of hydrogen peroxide under the synergistic electrocatalysis of AuNPs, CdTe–CdS and G–AuNP on the surface of the modified electrode.

3.3. Electrochemical response of the biosensor to hydrogen peroxide

The CVs of the as-prepared biosensor in the absence and presence of 1×10^{-8} M hydrogen peroxide in pH 7.0 PBS are shown in Fig. 4. As can be seen, after addition of hydrogen peroxide, the cathodic and anodic peak current increased dramatically, indicating catalytic properties of the modified electrode towards hydrogen peroxide. Because the reduction current responses are higher than the oxidization current responses, hydrogen peroxide concentration was determined by monitoring the increase in the reduction peak current of the biosensor.

The catalytic mechanism of the immobilized HRP towards hydrogen peroxide can be explained by the Scheme 1. As shown in the Scheme 1, the HRP immobilized on the modified electrode reacts with hydrogen peroxide to form a first intermediate (Compound I), which is a two-equivalent oxidized form containing an oxyferryl heme (Fe^{4+}=O) and a porphyrin π cation radical. Compound I shows catalytic activity, and its porphyrin radical abstracts one electron from the electrode to form a second intermediate (Compound II), which is subsequently reduced back to the native HRP by accepting one electron from the electrode [26]. During above process, the synergistic contributions of G–AuNP, CdTe–CdS and AuNPs as nanocomposite mediator improve the electron relay for activation of oxidation of hydrogen peroxide, which would accelerate electrochemical reaction and results a high enzyme activity and rapid response to hydrogen peroxide.

3.4. Effect of pH

The pH value of the electrolyte is important to performance of the biosensor because activity of the enzyme is affected greatly by acidity of the medium. The results showed the CV peak current response of the biosensor at different pH values in the presence of the same concentration of hydrogen peroxide. The response current increased from pH 5.0 and reached the maximum at pH 7.0, then decreased to pH 7.5. Strongly acidic or alkaline environments would result in the denaturation of enzyme. Therefore, pH 7.0 is selected as the optimized value for the HRP.

3.5. Calibration, linearity and detection limit

The calibration curve of hydrogen peroxide in pH 7.0 PBS was measured by differential pulse voltammetry. As shown in

$$\text{HRP } (Fe^{3+}) + H_2O_2 \rightarrow \text{Compound I } (Fe^{4+}{=}O) \quad (1)$$

$$\text{Compound I } (Fe^{4+}{=}O) + e^- + H^+ \rightarrow \text{Compound II} \quad (2)$$

$$\text{Compound II} + e^- + H^+ \rightarrow \text{HRP } (Fe^{3+}) + H_2O \quad (3)$$

Scheme 1. The catalytic mechanism of the immobilized HRP towards hydrogen peroxide.

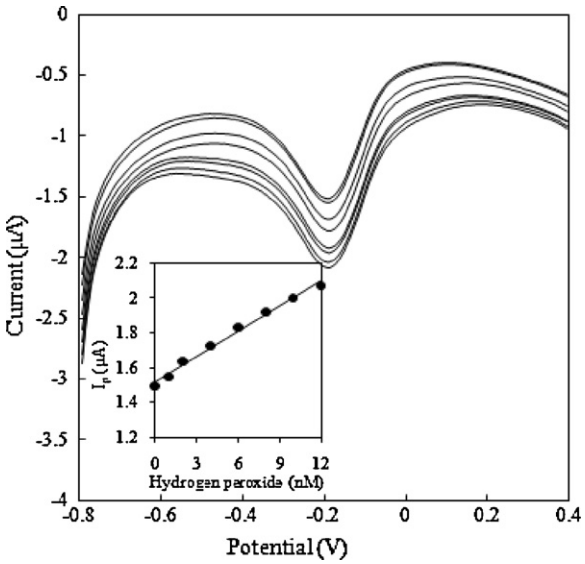

Fig. 5. Differential pulse voltammograms for the determination of HRP/AuNPs/CdTe–CdS/G–AuNP/GE to sequential addition of a series of hydrogen peroxide concentration from 0.0 M to 12 nM. Inset: Calibration plot of concentration of hydrogen peroxide vs. peak current.

Fig. 5, the anodic peak current of hydrogen peroxide was linearly related to the concentration over the range from 1×10^{-10} M to 1.2×10^{-8} M. The linear regression equation was I_{pa} (μA) = 0.0482C (nM) + 1.52, with a correlation coefficient of R = 0.9993. The detection limit (S/N = 3) was 3.2×10^{-11} M that was obtained from the signal-to-noise characteristics of these data (S/N = 3), which is obviously better than other hydrogen peroxide biosensors based on graphene materials such as Au–graphene–HRP–chitosan biocomposites (1.7×10^{-6} M) [12], cationic polyelectrolyte-functionalized graphene/gold nanoparticles (2.2×10^{-7} M) [27], single-layer graphene nanoplatelet–enzyme composites (1.05×10^{-7} M) [28], Ag/graphene composites (2.8×10^{-7} M) [29], MnO_2/graphene oxide nanocomposite [30], and graphene modified basal-edge plane pyrolytic graphite [31].

3.6. Functions of G–AuNP, CdTe–CdS and AuNPs

To understand functions of the G–AuNP, CdTe–CdS and AuNPs, four hydrogen peroxide biosensors were well fabricated by the same procedure described in Section 2.4, including the HRP/AuNPs/CdTe–CdS/G–AuNP/GE, HRP/AuNPs/CdTe–CdS/GE (only without G–AuNP), HRP/AuNPs/G–AuNP/GE (only without CdTe–CdS) and HRP/CdTe–CdS/G–AuNP/GE (only without AuNPs). Then, their analytical characteristics were well investigated by differential pulse voltammetry. It was found that the detection limits are 3.2×10^{-11} M for the HRP/AuNPs/CdTe–CdS/G–AuNP/GE, 3.6×10^{-10} M for the HRP/AuNPs/CdTe–CdS/GE, 6.6×10^{-11} M for the HRP/AuNPs/G–AuNP/GE and 5.1×10^{-11} M for the HRP/CdTe–CdS/G–AuNP/GE, indicating that the sensitivity of HRP/AuNPs/CdTe–CdS/G–AuNP/GE is higher than 11-fold that of HRP/AuNPs/CdTe–CdS/GE, 2-fold that of HRP/AuNPs/G–AuNP/GE and 1.6-fold that of HRP/CdTe–CdS/G–AuNP/GE. These results showed the each nanomaterial is very important to improve sensitivity of the biosensor.

High sensitivity of the biosensor (HRP/AuNPs/CdTe–CdS/G–AuNP/GE) should be attributed to unique surface architecture. First, the CdTe–CdS, located middle of the surface architecture, acts as an electron transfer channel between G–AuNP and AuNPs. As the CdTe–CdS offers an ultrafast charge carrier and charge transfer, the relay of electron transfer is very efficient and rapid. Moreover, particular alignment of conduction and valence band of the CdTe–CdS creates favoring electron transfer between CdTe–CdS and AuNPs or G–AuNP [32]. Second, the AuNPs, located outside of the surface architecture, was used to immobilize the HRP and facilitate electron transfer between the HRP and CdTe–CdS [22]. When oxidation of the redox carry out on the surface of the modified electrode, the AuNPs act as "donor" of the electron and rapidly pushes the electron towards the CdTe–CdS, in which the CdTe–CdS acts as "acceptor" of the electron and pulls the electron towards the CdTe–CdS. Above push and pull activities will accelerate the electron transfer between the AuNPs and CdTe–CdS, as well as the hole transfer in the CdTe–CdS [33]. Third, the G–AuNP, located inside of the surface architecture, will enhance the electron transport between G–AuNP and CdTe–CdS, and suppress the recombination of electron–hole pair in the CdTe–CdS due to large specific electronic conjugate system [34,35]. When oxidation of the redox carry out on the surface of the modified electrode, the G–AuNP acts as "acceptor" of the electron and rapidly pulls the electron towards the G–AuNP, in which CdTe–CdS acts as "donor" of the electron and pushes the electron towards the G–AuNP. The push and pull activities will accelerate the electron transfer between G–AuNP and CdTe–CdS, and the hole transfer in the CdTe–CdS. In conclusion, the combination of above three factors brings an electrocatalytic synergy towards hydrogen peroxide.

3.7. Reproducibility and stability

The reproducibility and stability of the biosensor were performed by measuring the current response of the biosensor upon 1.0×10^{-8} M of hydrogen peroxide. The average relative standard deviation was not more than 1.22% for ten successive determinations using the same biosensor, and 2.3% for six different biosensors which were fabricated independently by the same procedure described in Section 2.4, indicating the good reproducibility of the method. The as-prepared biosensor was stored in air at an ambient conditions, the current response was recorded each week. It was found that the peak current response at differential pulse voltammetry is approximately 97.2% of the originally measured value after 20 weeks. The fact shows good long-term stability and sensitivity for the analysis of real samples.

3.8. Interferences study

The influence of electrochemical interference to hydrogen peroxide on the current response of the biosensor was evaluated. The results indicated the injection of 100-fold ascorbic acid and 100-fold uric acid did not influence the current response of hydrogen peroxide (1.0×10^{-8} M). Electrochemical detection of hydrogen peroxide was possible at a lower potential due to the synergistic electrocatalytic influences of AuNP, CdTe–CdS and G–AuNP. Hence, there is negligible interference from other electro-active components.

4. Conclusions

The electrocatalytic synergy of G–AuNP, CdTe–CdS and AuNPs remarkably improves the electron relay and accelerates the electrochemical reaction, and AuNPs–CS film offers favorable microenvironment to keep bioactivity of the HRP. The as-prepared biosensor provides the best sensitivity in all biosensors based on graphene materials for detection of hydrogen peroxide up to now. This study also opens up a new challenge and approach to explore the electrochemical features of graphene or its nanocomposites for the potential utilizations.

Acknowledgements

The authors acknowledge the financial support from the National Natural Science Foundation of China (20771045), Natural Science Foundation of Zhejiang Province (Y4100729), National Science and Technology Support Project (2011BAK10B03) and sponsored by Qing Lan Project.

References

[1] K.S. Novoselov, A.K. Geim, S.V. Morozov, D. Jiang, Y. Zhang, S.V. Dubonos, I.V. Grigorieva, A.A. Firsov, Science 306 (2004) 666–669.
[2] K.I. Bolotin, K.J. Sikes, Z. Jiang, M. Klima, G. Fudenberg, J. Hone, P. Kim, H.L. Stormer, Solid State Commun. 146 (2008) 351–355.
[3] C. Wang, L. Zhang, Z.H. Guo, Microchim. Acta 169 (2010) 1–6.
[4] M. Matsushiraa, H. Uchida, G. Kalita, J. Mater. Chem. 20 (2010) 9713–9717.
[5] Z.F. Du, X.M. Yin, M. Zhang, Q.Y. Hao, Y.G. Wang, T.H. Wang, Mater. Lett. 64 (2010) 2076–2979.
[6] R. Louie, MRS Bull. 33 (2008) 1133.
[7] H.J. Du, J.S. Ye, J.Q. Zhang, X.D. Huang, C.Z. Yu, J. Electroanal. Chem. 650 (2011) 209–213.
[8] S.H. Goh, M. Pumera, Anal. Chem. 82 (2010) 8367–8370.
[9] Z. Jin, D. Nackashi, W. Lu, C. Kittrell, J.M. Tour, Chem. Mater. 22 (2010) 5695–5699.
[10] C.S. Shan, H.F. Yang, D.X. Han, Q.X. Zhang, A. Ivaska, L. Niu, Biosens. Bioelectron. 25 (2010) 1070–1074.
[11] Ch.P. Fu, Y.F. Kuang, Z.Y. Huang, X. Wang, N. Du, J.H. Chen, H.H. Zhou, Chem. Phys. Lett. 499 (2010) 250–253.
[12] K.F. Zhou, Y.H. Zhu, X.L. Yang, J. Luo, C.Z. Li, S.R. Luan, Electrochim. Acta 55 (2010) 3055–3060.
[13] H. Wu, J. Wang, X.H. Kang, Ch.M. Wang, D.H. Wang, J. Liu, I.A. Aksay, Y.H. Lin, Talanta 80 (2009) 403–406.
[14] F. Liu, J.Y. Choi, T.S. Seo, Chem. Commun. 46 (2010) 2844–2846.
[15] Y. Zhou, S. Liu, H.J. Jiang, H. Yang, H.Y. Chen, Electroanalysis 22 (2010) 1323–1326.
[16] M.H. Yang, B.G. Choi, H. Park, W.H. Hong, S.Y. Lee, T.J. Park, Electroanalysis 22 (2010) 1223–1228.
[17] L.V. Zhang, L.W. Yin, C.X. Wang, J. Phys. Chem. C 114 (2010) 9651–9658.
[18] P.M.A. Farias, A. Fontes, A. Galembeck, R.C.B.Q. Figueiredo, B.S. Santos, J. Brazil. Chem. Soc. 19 (2008) 352–356.
[19] Y.C. Wang, H. Mao, L.B. Wong, Nanotechnology 21 (2010), 055101:1–055101:7.
[20] B. Chon, J. Bang, J. Park, J. Phys. Chem. C 115 (2011) 436–442.
[21] S.W. Kim, B. Kim, S. Kim, J. Park, T. Kim, E. Jang, S. Jun, H. Jang, Small 7 (2011) 70–73.
[22] C.L. Li, Y. Su, X.Y. Lv, H.L. Xia, Y.J. Wang, Sens. Actuators B: Chem. 149 (2010) 427–431.
[23] J. Wang, Y.T. Long, Y.L. Zhang, X.H. Zhong, L.Y. Zhu, Chemphyschem 10 (2009) 680–685.
[24] W.S. Hummers, R.E. Offeman, J. Am. Chem. Soc. 80 (1958) 1339–1342.
[25] N.I. Kovtyukhova, P.J. Ollivier, B.R. Martin, T.E. Mallouk, S.A. Chizhik, E.V. Buzaneva, A.D. Gorchinskiy, Chem. Mater. 11 (1999) 771–776.
[26] Y. Xiao, H.Y. Chen, H.X. Ju, Anal. Biochem. 278 (2000) 22–28.
[27] Y. Fang, S. Guo, C. Zhu, Y. Zhai, E. Wang, Langmuir 26 (2010) 11277–11282.
[28] Q. Lu, X. Dong, L.J. Li, X. Hu, Talanta 82 (2010) 1344–1348.
[29] S. Liu, J.Q. Tian, L. Wang, H.L. Li, Y.W. Zhang, X.P. Sun, Macromolecules 43 (2010) 10078–10083.
[30] L. Li, S. Liu, Q. Hao, Y. Wang, Q. Li, T. Wang, Z. Du, Talanta 82 (2010) 1637–1642.
[31] W.J. Lin, C.S. Liao, J.H. hang, Y.C. Tsai, Electrochem. Commun. 11 (2009) 2153–2156.
[32] S. Rawalekar, S. Kaniyankandy, S. Verma, H.N. Ghosh, J. Phys. Chem. C 114 (2010) 1460–1466.
[33] A.D. Quach, G. Crivat, M.A. Tarr, Z. Rosenzweig, J. Am. Chem. Soc. 133 (2011) 2028–2030.
[34] Jia, D.H. Wang, Y.X. Huang, A.W. Xu, H.Q. Yu, J. Phys. Chem. C, doi:10.1021/jp2023617.
[35] H.B. Yang, G.H. Guai, C.X. Guo, Q.L. Song, S.P. Jiang, Y.L. Wang, W. Zhang, C. M. Li, J. Phys. Chem. C, doi:10.1021/jp201178a.